Applied Catalysis B: Environmental 90 (2009) 677–687

Contents lists available at ScienceDirect

Applied Catalysis B: Environmental

journal homepage: www.elsevier.com/locate/apcatb

TiO_2/Na-HZSM-5 nano-composite photocatalyst: Reversible adsorption by acid sites promotes photocatalytic decomposition of methyl orange

Peng Guo, Xiangsheng Wang, Hongchen Guo *

State Key Laboratory of Fine Chemicals, Department of Catalytic Chemistry and Engineering, Dalian University of Technology, Zhongshan Street 158, Dalian 116012, China

ARTICLE INFO

Article history:
Received 24 January 2009
Received in revised form 27 April 2009
Accepted 29 April 2009
Available online 6 May 2009

Keywords:
TiO_2/Na-HZSM-5 nano-composite photocatalyst
Reversible adsorption
Acid site
MO photodegradation

ABSTRACT

TiO_2/Na-HZSM-5 nano-composite photocatalysts were prepared by dispersing TiO_2 onto the external surface of Na^+-modified nano-ZSM-5 zeolite using a sol–gel process. Samples were characterized by XRF, XPS, HRTEM, XRD, DRUV–vis, NH_3-TPD, FT-IR, and the adsorption and photodegradation of methyl orange (MO) in aqueous solution. Results show the modification of support by Na^+ does not affect the loading, dispersion and structure of loaded TiO_2, but reduces the acidity of the nano-zeolitic support by preferentially eliminating stronger acid sites. The MO adsorption mainly takes place on the external surface of the supports. The strong and medium strong acid sites of the supports are the adsorption sites. MO molecules adsorbed by strong acid sites are difficult to desorb, whereas the adsorption of MO by medium strong acid sites is reversible. Generally, the MO photodegradation activity of TiO_2/Na-HZSM-5 nano-composites is better than that of bare TiO_2. However, it changes remarkably with the Na^+ content of the supports, giving the maximum value at 1.1 wt.% Na^+ when the MO adsorption by the support is almost completely reversible. The enhancement of the photodegradation activity of TiO_2/Na-HZSM-5 nano-composites is attributed to the reversible adsorption of MO by the medium strong acid sites on the nano-zeolitic supports.

1. Introduction

TiO_2-based photocatalysts have been extensively investigated in order to achieve better photocatalytic efficiency for a lot of attractive applications such as the decomposition of various organic pollutants in water and air. In recent years, studies on the doping of transition metal elements and nonmetal elements into TiO_2 and the dispersion of TiO_2 on supports have become attractive in the area of photocatalysis [1–4]. It is well known that TiO_2 photocatalysis relies on the electron–hole pairs generated in the conduction band and valence band of TiO_2 semiconductor. However, due to a relatively large band gap of ca. 3.20 eV (the position of UV absorption edge at around 380 nm), the generation of electron–hole pairs in bare TiO_2 is difficult and needs UV light irradiation which takes only about 2–3% of the solar light that reaches the earth. Besides, the recombination rate of electron–hole pairs in bulk TiO_2 particles is higher than that in fine TiO_2 particles [5–8]. As a result, the photocatalytic activity of the bulk TiO_2 particles is lower than that of the fine TiO_2 particles. What is more, the bare TiO_2 generally has very small adsorption capacity; such an inherent disadvantage makes it less efficient in remedying gas or water systems polluted by extremely dilute hazardous substances. Therefore, the current efforts in heteroatom doping is to narrow the band gap of TiO_2 for extending its photoresponse to visible light region, while the dispersion of TiO_2 on solid supports is to make TiO_2 in fine particles and to usher in the supports' adsorption ability as well. Certainly, the dispersion of TiO_2 on solid supports also facilitates the recovery of photocatalyst, for example, from huge volume of treated water, which can be troublesome and costly if fine TiO_2 particles are used directly [9].

The dispersion of TiO_2 has been tried with glass [6,10], stainless steel [11], alumina [7,12], silica [7,12–15], multi-oxides $Ce_{0.5-x}Zr_{0.5-x}Ba_{2x}O_2$ [16], activated carbons [17–21], carbon nanotubes [22,23], mesoporous molecular sieves MCM-41 [24–27], and zeolites [8,9,12,25–39], etc. Except for a few negative examples [32], the dispersion of TiO_2 on supports successfully increases the photocatalytic activity of TiO_2 to some extent. A commonly observed effect of TiO_2 dispersion is the blue shift of TiO_2 absorption edge in ultraviolet region, which is regarded as the size quantization effect of fine TiO_2 particles. In addition, many researchers concluded that the adsorption of support also contributed to the photocatalytic efficiency enhancement of dispersed TiO_2 [5,8,18,25–27,32,33,35,38]. The adsorption of substrate by supports should have profound meaning in developing TiO_2-based photocatalysis. This is easy to understand in view of the fact that the dilute hazardous substances in either liquid-phase

* Corresponding author. Tel.: +86 411 39893913; fax: +86 411 83689065.
E-mail address: hongchenguo@163.com (H. Guo).

0926-3373/$ – see front matter © 2009 Elsevier B.V. All rights reserved.
doi:10.1016/j.apcatb.2009.04.028

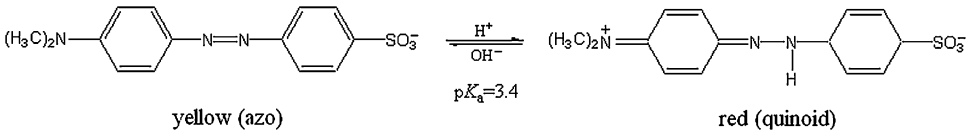

Scheme 1. Molecular structures of methyl orange (MO) molecule.

or gas-phase systems can be concentrated to the vicinity of supported TiO_2 photoactive sites by supports.

The adsorption of organic compounds on zeolites has been considered occurring through van der Waals interactions with lattice oxygens of zeolitic crystal, or electrostatic interactions and π–π interactions with extraframework cations [8]. A relationship of zeolitic surface hydrophobicity with its adsorption towards organic substrates has also been mentioned [5,25,31]. Most recently, Anpo and coworkers [38] studied the effect of hydrophobicity of zeolites on the adsorption and photocatalytic decomposition of acetaldehyde in detail. They observed that in the composite of TiO_2 and hydrophobic H-ZSM-5 zeolite (SiO_2/Al_2O_3 = 1880), the adsorption of acetaldehyde molecules was highly favored, and the composite gave high photocatalytic activity. While, in the composite of TiO_2 and hydrophilic H-ZSM-5 zeolite (SiO_2/Al_2O_3 = 23.8), the adsorption of acetaldehyde molecules was disfavored, and the composite produced low photocatalytic activity. In view of the crystal structure diversity of zeolitic materials (more than 179, different crystal structures determine different capillary pore sizes, specific pore volumes and specific surface areas), the feasibility of isomorphous substitution of their framework Si and Al atoms with a number of heteroatoms such as B, Ga, Ge, P, Ti, V, Cr, Fe, etc. (the change of framework composition will modify the electronegativity of lattice oxygen ions), and the ion-exchangeability of their original extraframework cations, usually alkaline metal cations, by NH_4^+, H^+, alkaline-earth metal cations, transitional metal cations, and rare-earth metal cations (the ion-exchange will change zeolitic acidity and electrostatic field), it is possible to efficiently adsorb different organic compounds in both gas and water by using proper zeolitic supports. However, to facilitate photocatalysis, the adsorption sites of the zeolitic support and the photoactive sites of TiO_2 should appear in the same area, and the interaction force of adsorption sites with organic compounds should be at such a suitable strength level that the subsequent migration of the adsorbates to the photoactive sites can be guaranteed. These requirements highlight the necessity of providing a purpose-made zeolitic support for TiO_2 in a given photocatalytic application. Some authors have mentioned that the weak adsorption of organic compounds by supports favored the photocatalysis of supported TiO_2 [17,27,33]. The most recent paper [38] indicated that, the adsorption of acetaldehyde molecules on the silanol groups of HZSM-5 zeolite was weak adsorption, which promoted the photocatalytic decomposition of acetaldehyde by allowing the absorbed species to spillover onto neighboring TiO_2 sites quickly; whereas the adsorption of acetaldehyde molecules on sodium ions of NaZSM-5 zeolite was strong adsorption, which inhibited the photocatalysis. However research work on how to tailor a zeolitic support for TiO_2 composite photocatalyst has not been well investigated so far.

This paper concerns the photocatalytic decomposition of methyl orange (MO) over nano-composite photocatalysts, which are prepared by dispersing TiO_2 on a series of Na^+-modified nano-sized HZSM-5 zeolites. Focuses are given to the adsorption capacity of MO on the nano-zeolitic support, the nature of MO adsorption sites and the way to synergizing the photocatalysis of TiO_2 by the adsorption of support. MO is a good example of azo dyes and alkaline organic pollutants, and it is nonbiodegradable. Moreover MO is a well-known Hammett indicator for solid acidity titration [40,41]; the protonation of MO will make its color change from yellow (alkaline color) to red (acidic color) as shown in Scheme 1. Therefore, the use of MO photodegradation as probe reaction may offer the chance to observe the adsorption effect if the MO adsorption takes place on the acid sites of the zeolite. Besides, our motive for using nano-sized zeolite support is to disperse TiO_2 on the external surface of zeolite, so as to avoid the diffusion resistance of MO in ZSM-5 micropores (about 0.52–0.58 nm in diameter). Compared with its micro-sized counterpart, nano-sized zeolite has much larger external surface area, which would permit TiO_2 to have better dispersion at high loadings, while leaving the support enough uncovered external surface for MO adsorption.

2. Experimental

2.1. Photocatalyst preparation

Nano-sized NaZSM-5 (SiO_2/Al_2O_3 = 28.6 (mol), crystal size = ~50 nm, S_{BET} = 352.9 m^2/g) was hydrothermally synthesized in the presence of n-butylamine template [42]. Before used as a support, the as-synthesized zeolitic material was subjected to, firstly, a temperature-programmed calcination (473 K × 1 h → 573 K × 1 h → 673 K × 1 h → 773 K × 2 h → 813 K × 4 h) in a muffle furnace in the presence of air to remove the organic template, then twice repeated H^+-exchanges in a solution of 0.6 M HNO_3 (ambient condition, 1 h for each time, solid–liquid ratio = 1:10, g/ml), and last drying (383 K, overnight) and calcination (813 K, 3 h) treatments to obtain protonic acid nano-HZSM-5 (SiO_2/Al_2O_3 = 31.5 (mol), S_{BET} = 363.5 m^2/g). The protonic acid zeolite was further dipped with $NaNO_3$ aqueous solutions of different concentrations to obtain Na^+-impregnated zeolitic supports of 0.1, 0.6, 1.1, 1.3, 1.7, 2.1, 2.6 wt.% Na^+ content, respectively. The dipping operations were conducted at 353 K for 1 h using a fixed solid–liquid ratio of 1:4 (g/ml). The solids were recovered from solution by vacuum filtering, dried at 383 K overnight, and calcined at 813 K for 3 h to obtain the supports. These supports were denoted as χNa-HZSM-5, where χ is the Na content in weight percent.

The dispersion of TiO_2 onto nano-sized χNa-HZSM-5 zeolitic supports was performed according to a sol–gel process, which was featured by dipping the zeolitic support with an absolute ethanol–diethanolamine solution that contained butyltitanate ($Ti(OBu)_4$) at ambient conditions for 4 h, under continuous magnetic stirring. Water consumed by the hydrolysis of $Ti(OBu)_4$ was supplied by the pre-absorbed water in the micropores of the nano-sized zeolite. In this way the hydrolysis of $Ti(OBu)_4$ and the subsequent sol–gel process of TiO_2 were slowed down by the slow release of H_2O from the zeolitic micropores, which was expected to be helpful for inhibiting the excessive aggregation of TiO_2 gel particles. The solid product was recovered by plain sedimentation. It was dried at 343 K overnight, and calcined in air at 773 K for 1 h to obtain the TiO_2/χNa-HZSM-5 composite photocatalysts. Reagents used, such as butyltitanate, diethanolamine and absolute ethanol, were all of analytical grade. For the purpose of comparative photocatalysis study, bare nano-sized TiO_2 was also prepared using a reported method [43].

2.2. Photocatalyst characterization

Bulk chemical composition was determined with Bruker SRS-3400 sequential X-ray fluorescence (XRF) spectrometer. Surface

elemental composition and elemental chemical state were measured by X-ray photoelectron spectra (XPS) using Thermo VG ESCALAB250 photoelectron spectrometer (Mg Kα radiation, operated at 300 W). The shift of binding energy due to relative surface charging was calibrated using C1s level at 284.6 eV as an internal standard. Crystal structure was analyzed by Rigaku D/Max-2400 powder X-ray diffractometer (XRD, Cu Kα radiation, λ = 1.5406 Å). Particle size of supported TiO_2 was observed by Tecnai G^2 20 S-twin high-resolution transmission electron microscopy (HRTEM, acceleration voltage of 200 kV). Diffuse reflectance UV–vis spectra were obtained on a JASCO UV-550 spectrometer with $BaSO_4$ as reference. Catalyst acidity was determined by the NH_3 temperature-programmed desorption (NH_3-TPD) technique, and the pyridine adsorption Fourier-transition infrared (FT-IR) spectroscopy with a Bruker EQUINOX55 FT-IR spectrometer.

2.3. Photocatalyst adsorption behavior characterization

The adsorption capacities of different photocatalysts were assessed by monitoring, in the dark, the equilibrium concentration of a MO aqueous solution that contacted the photocatalysts. The reversible adsorption behavior of the photocatalysts was investigated by monitoring, in the dark, the change of the equilibrium concentration of the MO aqueous solution that contacted the photocatalysts during a stepwise increase/decrease of the temperature of MO solution. The aqueous solution used for the abovementioned purpose had an initial MO concentration of 20 mg/l. The ratio of solution to photocatalyst was fixed at 100/1 (ml/g). The MO concentration was monitored by the absorbance of MO at 464 nm with a homemade PC 22 visible spectrophotometer. To shorten the time needed for adsorption/desorption equilibrium, continuous magnetic agitation was applied in these experiments.

2.4. Photodegradation of methyl orange

The photocatalytic degradation of MO was carried out in a glass photoreactor shown in Fig. 1. The reaction setup was installed in an isolated cabin. The temperature of the reactor was controlled at 298 K by a water jacket. A 250 W homemade high pressure mercury lamp was employed as the ultraviolet light irradiation source. The lamp was placed 5 cm above the surface of MO solution. In a typical run, 1 g photocatalyst was suspended in 100 ml MO aqueous solution (20 mg/l). Under continuous magnetic agitation, one hour's dark adsorption of MO on photocatalyst was allowed to ensure the adsorption equilibrium of MO on the photocatalyst being reached, and then the ultraviolet light irradiation was given to start the photodegradation. The total irradiation time was 2 h for each run. At regular intervals, the suspension was sampled for MO concentration analysis, which was done by the same means as mentioned in foregoing adsorption section. The percentage of MO degraded was calculated according to the following expression:

$$\text{Degradation}\,(\%) = \frac{\begin{array}{l}\text{the amount of MO in initial solution}\\ -\text{ the amount of MO in final solution}\\ -\text{ the amount of MO on the solid}\\ \quad\text{photocatalyst}\end{array}}{\text{the amount of MO in initial solution}} \times 100$$

3. Results and discussion

3.1. Characterizations of the TiO_2/χNa-HZSM-5 composites

3.1.1. Chemical composition

XRF analysis indicates that the increase of Na^+ content in nano-HZSM-5 zeolite support has no influence on the loading of TiO_2 in the TiO_2/χNa-HZSM-5 composite (Fig. 2). Each sample contains around 9 wt.% TiO_2, approaching 50% of the maximum theoretical loading in our preparation system. XPS spectra in Fig. 3 show that the TiO_2/χNa-HZSM-5 composites roughly have the same peaks for binding energy of Ti2p1/2 and Ti2p3/2 as P25 TiO_2 and self-prepared TiO_2, indicating that TiO_2 dispersed on the nano-HZSM-5 zeolite has octahedrally coordinated anatase structure. Fig. 4 gives the XPS survey spectra for all detectable surface elements, among which we believe the C1s signal is caused by contamination. Table 1 shows that both XRF and XPS give similar Si/Al ratio for the nano-zeolitic supports, but Na^+ content and TiO_2 loading detected by XPS are about two times as much as those by XRF. This means that TiO_2 is mainly dispersed on the external surface of the nano-zeolitic support. It has been reported that the loading of TiO_2 on zeolites takes place on surface ≡Si–OH or/and ≡Al–OH [32,34,44–46]. In this case, the acidic ≡Al–OH hydroxyls on the external surface of nano-HZSM-5 zeolite were preferentially occupied by Na^+, as can be seen from later acidity characterization section, forming ≡Al–ONa. Judging from the insensibility of TiO_2 loading to the Na^+ content of the nano-zeolitic support, we speculate that the deposition of TiO_2 on the external surface of our zeolitic support in the sol–gel process could occur on sites other than surface ≡Si–OH or/and ≡Al–OH, such as Na^+ sites.

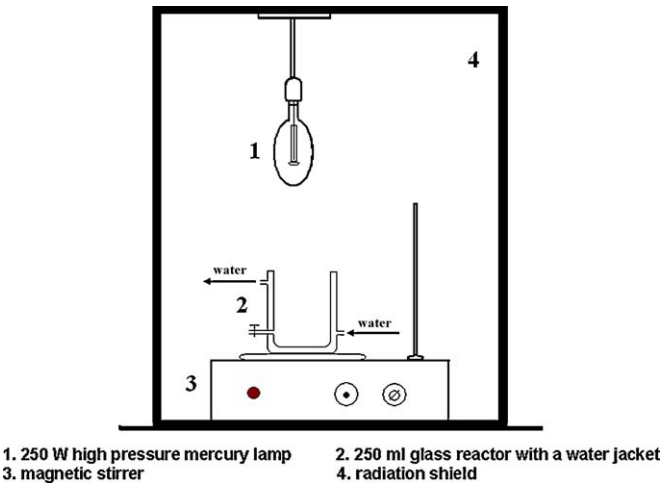

Fig. 1. Schematic drawing of the photoreactor.

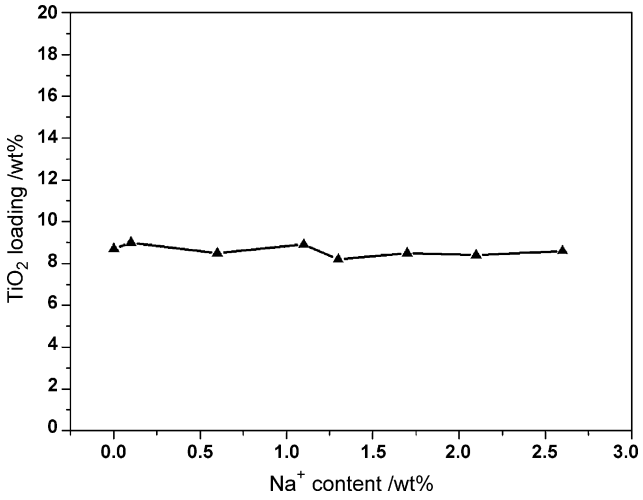

Fig. 2. XRF analysis for TiO_2 loadings and Na^+ contents in TiO_2/χNa-HZSM-5 composites.

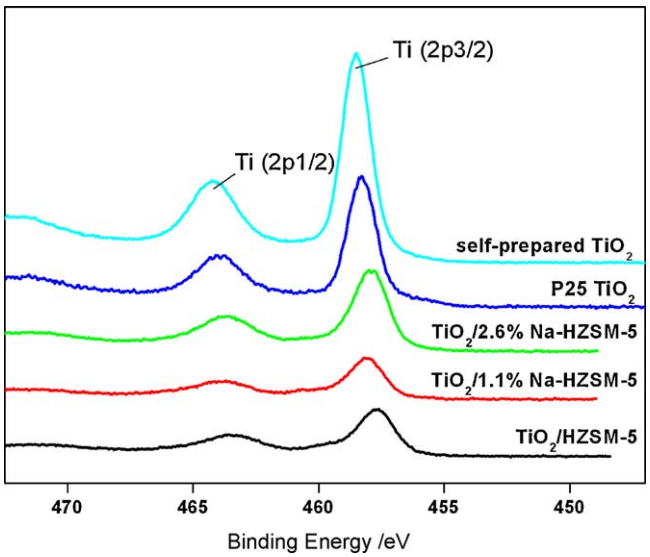

Fig. 3. XPS analysis for Ti2p of P25 TiO_2, self-prepared TiO_2 and TiO_2/χNa-HZSM-5 composites.

3.1.2. Particle size of the nano-zeolitic support and supported TiO_2

It is observed from TEM image in Fig. 5(A), that the particle size of the nano-zeolitic support is about 50 nm, and that the ultrafine zeolitic particles have a strong inclination to aggregate, indicating they have very high unsaturated surface energy. After being loaded with TiO_2, the aggregation tendency of the ultrafine zeolitic particles seems disappeared. As a result, the TEM image of TiO_2/HZSM-5 composite (Fig. 5(B)) has a great change, compared with that of nano-HZSM-5 zeolitic support (Fig. 5(A)). Obviously, the loading of TiO_2 has changed the surface property of the nano-HZSM-5 zeolitic support. HRTEM analysis suggests that TiO_2 dispersed on the external surface of the nano-HZSM-5 zeolitic support (Fig. 6(A)) is in the size range of not more than 10 nm (Fig. 6(B and C)). Therefore, the TiO_2/χNa-HZSM-5 composites were prepared as nano-composites.

3.1.3. Phase composition

XRD patterns of nano-HZSM-5 zeolitic support, self-prepared TiO_2 and TiO_2/χNa-HZSM-5 nano-composites are presented in Fig. 7. It shows that the dispersion of TiO_2 on nano-χNa-HZSM-5 does not damage the zeolite's MFI topology which is characterized by five main peaks at 2 theta equal to 7.95, 8.89, 23.18, 23.99, and 24.45 [47]. Although the TiO_2 was dispersed mainly on the external surface of the zeolitic support and in quite high loading (near 20 wt.% determined by XPS), practically no TiO_2 diffraction peak, neither anatase nor rutile, was detected. This result is in good agreement with HRTEM measurement which suggests the high dispersion of TiO_2 on the surface of the zeolitic support.

3.1.4. Photoresponse property

As shown by the DRUV–vis spectra in Fig. 8, all the nano-χNa-HZSM-5 zeolitic supports have very weak absorbance in ultraviolet region. And it is noted that, as Na^+ content increases, their absorbance in 190–260 nm region also slightly increases; this reason is still unknown. When these supports were loaded with about 9 wt.% TiO_2 (determined by XRF), the absorbance of the resulted TiO_2/χNa-HZSM-5 nano-composites dramatically increases in ultraviolet region, and the intensities of said absorbance in 190–320 nm are even stronger than that of bare nano-TiO_2. This suggests that the dispersion of TiO_2 on the nano-χNa-HZSM-5 supports has significantly increased the ultraviolet photoresponse of TiO_2. In addition, Fig. 8 also shows that all the TiO_2/χNa-HZSM-5 nano-composites have the same absorbance spectrum, and that the absorption edges of the nano-composites have equal shift towards shorter wavelength (viz. blue shift) compared with that of bare nano-TiO_2. The former is consistent with the forgoing conclusion that the Na^+ contents in the nano-χNa-HZSM-5 zeolitic supports almost have no influence on the dispersion of TiO_2, while the latter is an indicator of the reduction of TiO_2 particle size by supporting [46,48].

3.1.5. Acidity feature

HZSM-5 is a famous solid acid in heterogeneous catalysis area. The acidity of this kind of solid acid originates from the tetrahedrally coordinated framework aluminum sites which are able to offer protons (Brönsted acid), and from the electron-deficient sites, such as framework $\equiv Si^+$ sites and extraframework AlO^+ species, which are apt to accept a pair of electrons (Lewis acid). These acid sites can interact with reactants (act as alkalis) through chemisorption which is an indispensable step in solid acid catalysis. The acidic strength and acidic nature (Brönsted acid or Lewis acid) of a zeolitic acid can be measured by established methods like ammonia temperature-programmed desorption (NH_3-TPD) technique, and pyridine adsorption Fourier-transform infrared (FT-IR) spectroscopy technique. As shown in Fig. 9, the NH_3-TPD profile of the virginal nano-HZSM-5 zeolite is featured by two ammonia desorption peaks: the low-temperature peak (LTP) centered at around 523 K and the high-temperature peak (HTP) located at around 673 K, corresponding to weak and strong acid sites of the zeolite, respectively. After being loaded with TiO_2, the

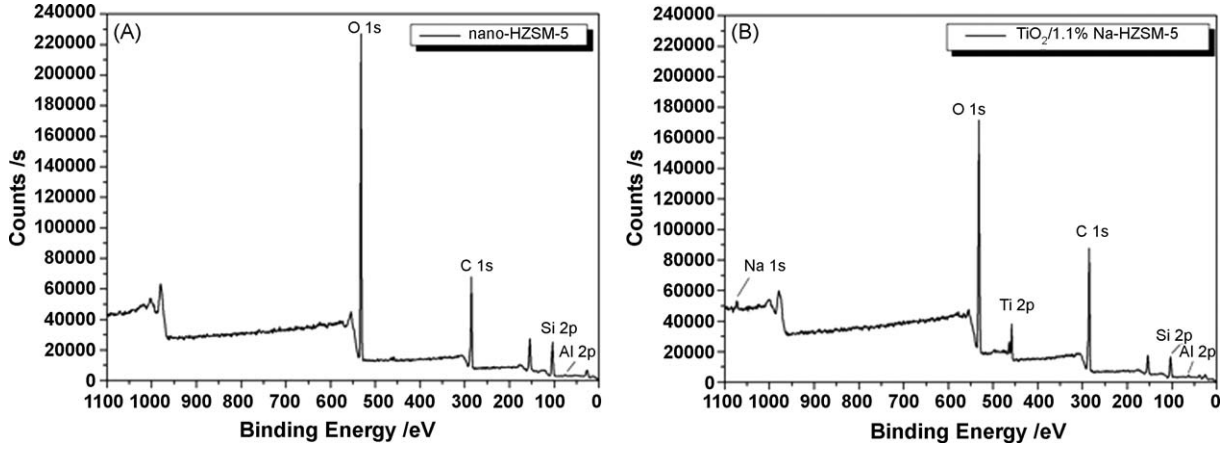

Fig. 4. XPS composition analyses for nano-HZSM-5 (A) and TiO_2/1.1%Na-HZSM-5 (B).

Table 1
Bulk and surface chemical compositions of three TiO_2/χNa-HZSM-5 composites determined by XRF and XPS methods.

Catalyst	XRF			XPS		
	Na^+ (wt.%)	Si/Al (mol)	TiO_2 (wt.%)	Na^+ (wt.%)	Si/Al (mol)	TiO_2 (wt.%)
TiO_2/HZSM-5	0	16.0	8.7	0	13.5	19.4
TiO_2/1.1%Na-HZSM-5	1.1	16.2	8.9	2.4	14.1	18.2
TiO_2/2.6%Na-HZSM-5	2.6	15.3	8.6	4.3	16.2	19.7

acidity distribution does not change obviously. However, as the Na^+ contents of the supports increase, the strong acid sites decrease in both bare supports and nano-composite catalysts; meanwhile the weak acid sites increase first and then decrease, displaying a maximum at χ = 1.3 wt.% (Fig. 10). The FT-IR spectra of the nano-χNa-HZSM-5 supports, shown in Fig. 11(A), are featured by three absorption peaks located at 1545 cm^{-1}, 1455 cm^{-1}, and 1490 cm^{-1}, respectively. The former two peaks are caused by the adsorption of pyridine on Brönsted acid sites and Lewis acid sites, respectively. The other one is caused by the absorption overlap of pyridine/Brönsted acid and pyridine/Lewis acid complexes. It is obvious that, by increasing Na^+ contents in the nano-χNa-HZSM-5 supports, the Brönsted acid sites decrease gradually due to the replacement of H^+ by Na^+; at the same time Lewis acid sites also show a decrease probably due to the formations of $\equiv SiO^-$–Na^+ and AlO_2^-–Na^+ structures from $\equiv Si^+$, AlO^+, NO_3^- and Na^+ via high-temperature solid-phase reactions. When the Na^+ content of the support increases to and beyond 1.3 wt.%, a new intensive absorption peak appears at 1444 cm^{-1}, which could be attributed to the formation of Na^+/pyridine complexes. This new absorption peak decreases in intensity and finally disappears when the outgassing temperature is elevated from 423 K to 723 K. This means that the Na^+ in the supports only act as weak Lewis acid sites. On the other hand, spectra recorded at different outgassing temperatures also disclose that the introduction of Na^+ into the nano-HZSM-5 zeolitic support preferentially eliminates strong acid sites, both Brönsted acid and Lewis acid, which is in line with the results of NH_3-TPD. After the loading of TiO_2, the resulted TiO_2/χNa-HZSM-5 composites show weaker intensity for every absorption peak at different outgassing temperatures than their corresponding supports. This phenomenon might be caused by the covering of the zeolitic external surface by the deposited TiO_2 nano-particles. By comparing Fig. 9 with Fig. 11, it can be found that the loading of TiO_2 on the nano-χNa-HZSM-5 zeolitic supports has little influence on the profiles of NH_3-TPD but very remarkable on the spectra of FT-IR. This might imply that the TiO_2 deposited onto the zeolitic external surface has partly blocked the pore-mouths of zeolitic supports, which prevents pyridine probe molecules (bulkier than NH_3 molecules) from entering the zeolitic pore channels. Besides, the little change of the NH_3-TPD profiles before and after TiO_2 loading also means that, the preparation of TiO_2/χNa-HZSM-5 composites has hardly disturbed the internal surface (pore channels) of the nano-χNa-HZSM-5 zeolitic supports. Therefore, the results of acidity characterizations agree with the forgoing conclusion from the chemical composition analyses that the TiO_2 is mainly dispersed on the external surface of nano-χNa-HZSM-5 zeolites.

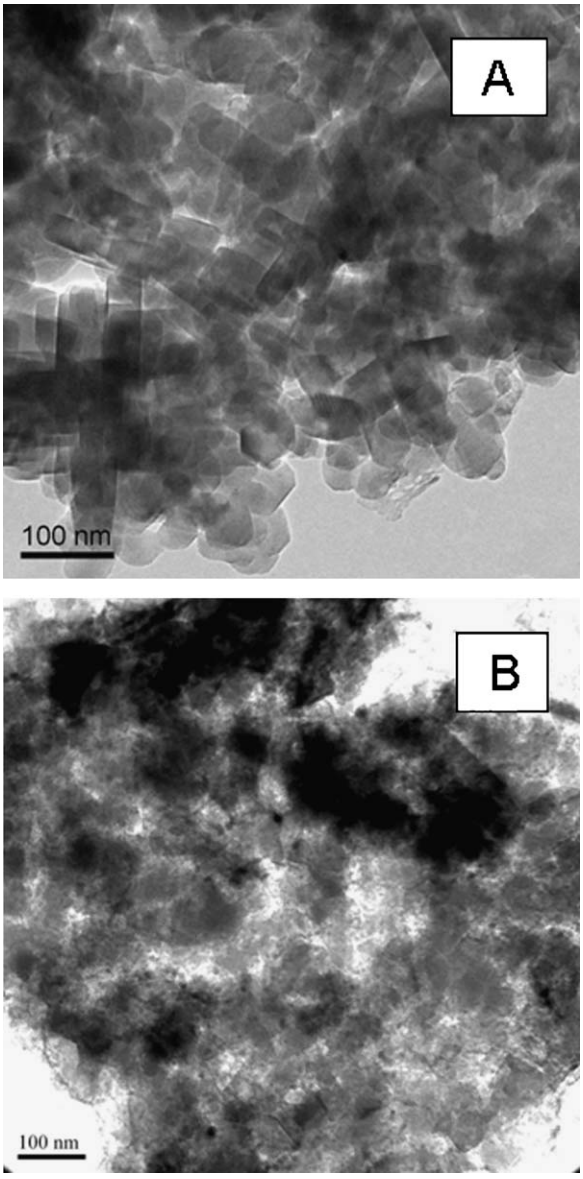

Fig. 5. TEM images of nano-HZSM-5 zeolitic support (A) and TiO_2/HZSM-5 composite (B).

3.2. Adsorption and photodegradation of MO on TiO_2/χNa-HZSM-5 nano-composites

From Fig. 12(A) it can be seen that, when contacted with MO solution in the dark, TiO_2/χNa-HZSM-5 nano-composites with different Na^+ contents show different adsorption capacities for MO substrate. TiO_2/HZSM-5 nano-composite (χ = 0) exhibits the biggest adsorption capacity, accounting for more than 40% of the total MO in the initial solution. As the Na^+ contents of the nano-χNa-HZSM-5 zeolitic supports increasing, the adsorption capacities of the corresponding TiO_2/χNa-HZSM-5 nano-composites decrease gradually; the TiO_2/2.6%Na-HZSM-5 nano-composite does not have obvious adsorption for MO substrate any more. Nevertheless, the Na^+-containing nano-composites do exhibit considerable adsorption capacities for MO at relatively low Na^+ contents. The adsorption equilibrium of MO on nano-composites arrives very quickly (within about 10 min), and then the concentration of MO solution ceases to change during the rest of one hour's dark experiment. After

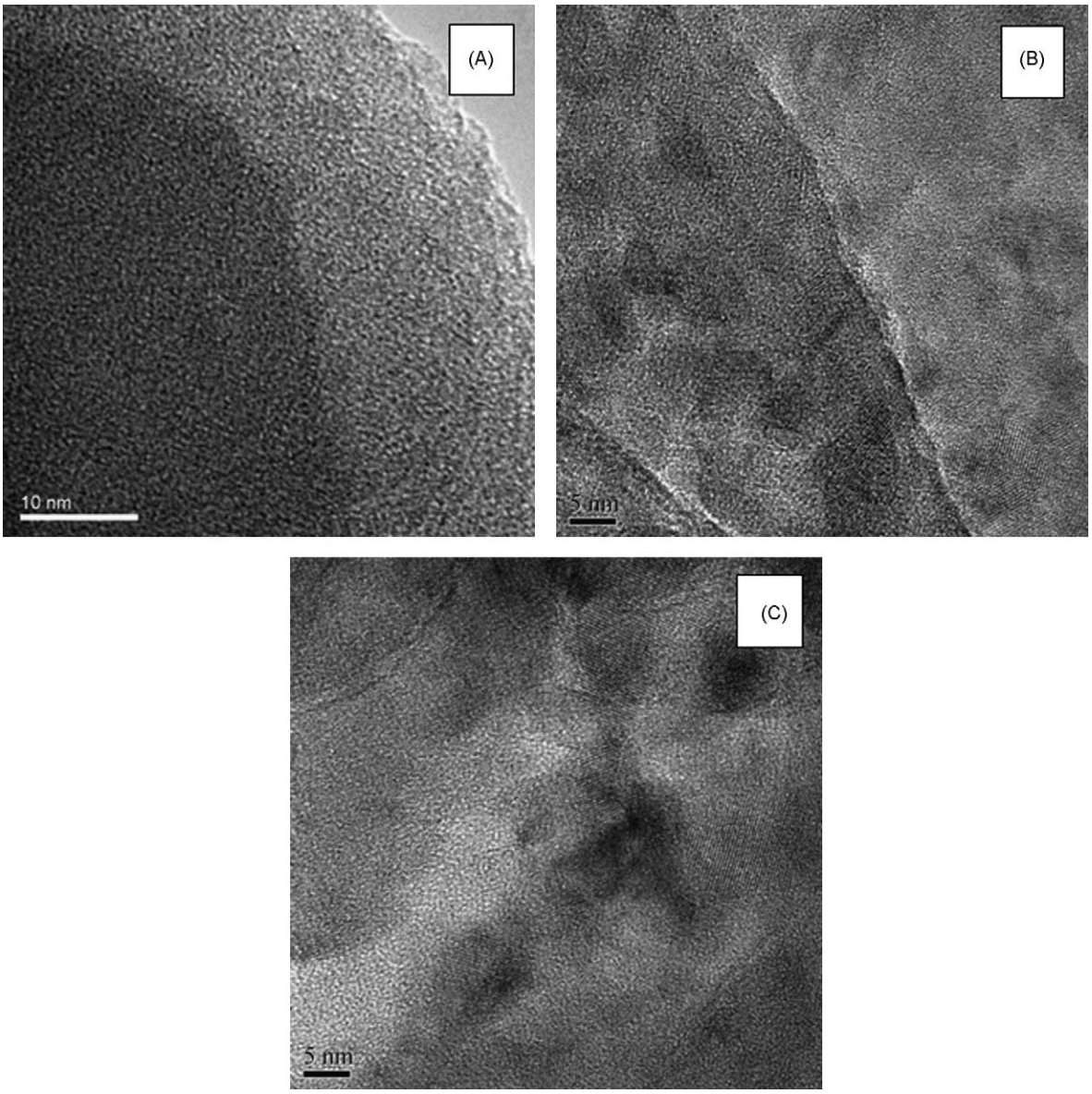

Fig. 6. Typical HRTEM images of nano-HZSM-5 zeolitic support (A) and TiO_2/χNa-HZSM-5 composites: TiO_2/HZSM-5 (B) and TiO_2/0.8%Na-HZSM-5 (C).

ultraviolet radiation is provided, however, the concentration of MO solution drops continuously over all TiO_2/χNa-HZSM-5 nano-composites. This proves that all the TiO_2/χNa-HZSM-5 nano-composites are effective photocatalysts for the degradation of MO. From Fig. 12(B) one can clearly find out that, as the Na^+ contents of the nano-χNa-HZSM-5 zeolitic supports being elevated, the MO adsorption capacities of the TiO_2/χNa-HZSM-5 nano-composites decrease, whereas the photocatalytic activities (MO degradation percentage) of the nano-composites increase first and then decrease. The maximum of the photocatalytic activity appears on TiO_2/1.1%Na-HZSM-5 nano-composite, which gives a MO adsorption capacity of 11.2% and a MO degradation percentage of 73.0%. It is observed that, on the basis of the same TiO_2 dosage, the photocatalytic activity of TiO_2/2.6%Na-HZSM-5 nano-composite is comparable to that of self-prepared bare TiO_2 (dashed line in Fig. 12(B)). It is interesting to mention that the TiO_2/2.6%Na-HZSM-5 nano-composite is also similar to the bare TiO_2 in term of poor adsorption capacity towards MO substrate.

The adsorption and photocatalysis behaviors of TiO_2/χNa-HZSM-5 nano-composites and bare TiO_2 lead us to such an idea: it is not the Na^+ itself but the adsorption property of the zeolitic support that affects the photocatalytic activity of supported TiO_2. On the other hand, the relationship of the Na^+ contents of χNa-HZSM-5 zeolitic supports with the acidity of the TiO_2/χNa-HZSM-5 nano-composites, as well as the alkaline essence of MO substrate, leads us to the assumption that MO substrate was absorbed on the acid sites of the zeolitic supports. If it was not, the absorbed MO would not display some red color according to Scheme 1 mentioned in Section 1. Cheeringly, the absorbed MO does display some red color, as shown in Fig. 13. According to the DRUV–vis spectra, MO solution has a characteristic absorption at about 460 nm. It belongs to the azo structure of MO, a chromophore producing yellow color. The adsorption of MO onto the TiO_2/χNa-HZSM-5 nano-composites makes the characteristic absorption shift to 500–525 nm. This new broad band belongs to the quinoid structure of MO, a chromophore producing red or magenta color. As the Na^+ content increasing, the broad band in 500–525 nm weakens. The photographs of the MO-absorbed TiO_2/χNa-HZSM-5 nano-composite photocatalysts (insert of Fig. 13) show that the colors of the TiO_2/χNa-HZSM-5 change from carmine to pale red as

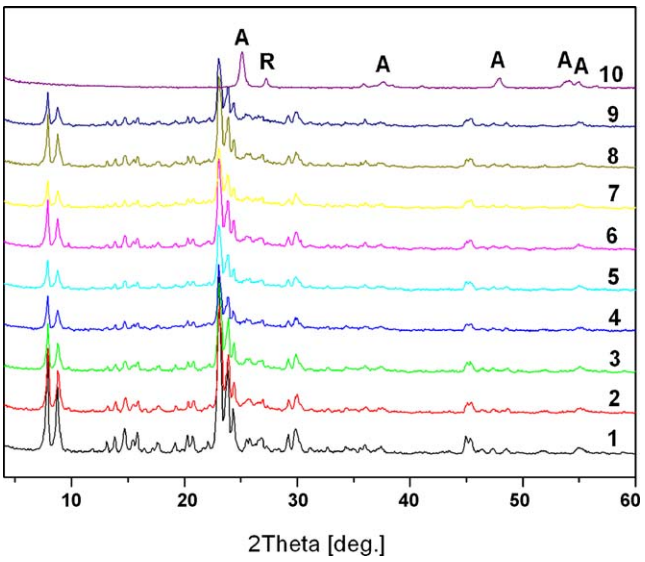

Fig. 7. XRD patterns of nano-HZSM-5 support (1), self-prepared TiO_2 (10), and TiO_2/χNa-HZSM-5 nano-composites (from 2 to 9, χ = 0, 0.1, 0.6, 1.1, 1.3, 1.7, 2.1, and 2.6 wt.%, respectively).

the Na^+ contents of the nano-χNa-HZSM-5 zeolitic supports increasing from 0 to 1.1 wt.%. Sample TiO_2/2.6%Na-HZSM-5, which is unable to absorb MO molecules and shows no characteristic absorbance for MO in the DRUV–vis spectrum, simply displays white color. Fig. 14 confirms that the adsorption of MO on TiO_2/χNa-HZSM-5 nano-composites preferentially takes place on relatively strong acid sites. The ineffectivity of TiO_2/2.6%Na-HZSM-5 in absorbing MO indicates that the weak acid sites on this nano-composite photocatalyst are too weak to absorb MO molecules. Thus, it is concluded that it is the external surface acidity of the zeolitic materials, not the pore structure of the zeolitic support, that plays an important role in enhancing the photocatalytic activity of TiO_2/χNa-HZSM-5. We have tested the possibility of other amorphous oxide supports for TiO_2 composite photocatalyst preparation. SiO_2 and Al_2O_3 were chosen because they are very popular supports for many petroleum processing/petrochemical catalysts. These oxides are featured by a quite broad distribution of pore size, generally ranging from micropores (less than 2 nm) to mesopores (2–50 nm) and macropores (more than 50 nm). Nevertheless, the TiO_2 composites prepared with them using the same sol–gel process showed very low MO adsorption capacities, and their MO photodegradation activities were not superior to the bare TiO_2, indicating that the loading of TiO_2 onto

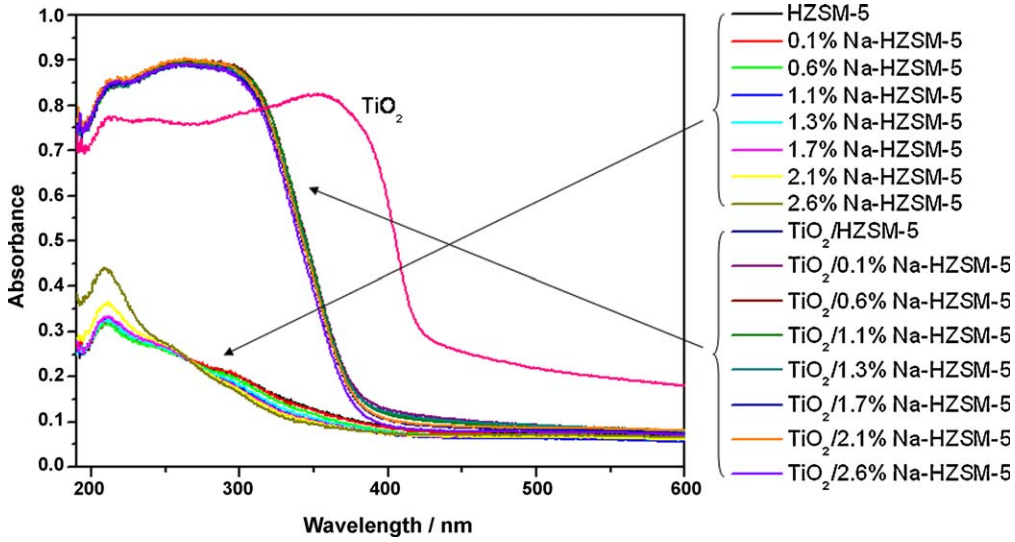

Fig. 8. DRUV–vis spectra of χNa-HZSM-5 and TiO_2/χNa-HZSM-5 nano-composites.

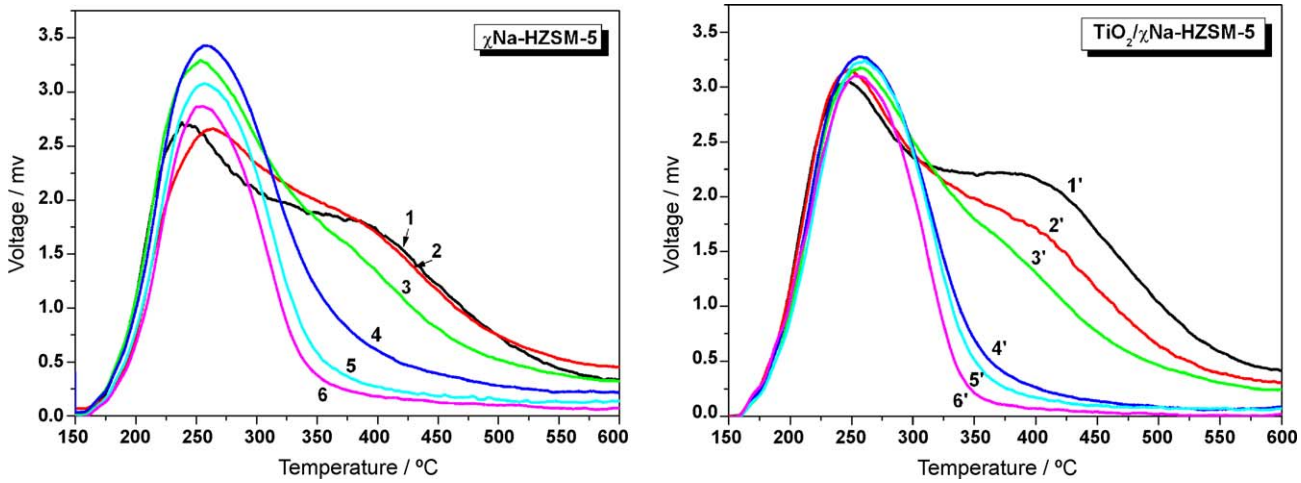

Fig. 9. NH_3-TPD profiles of χNa-HZSM-5 zeolites and TiO_2/χNa-HZSM-5 nano-composites, (1, 1′): χ = 0; (2, 2′): χ = 0.1; (3, 3′): χ = 0.6; (4, 4′): χ = 1.3; (5, 5′): χ = 2.1; (6, 6′): χ = 2.6 wt.%.

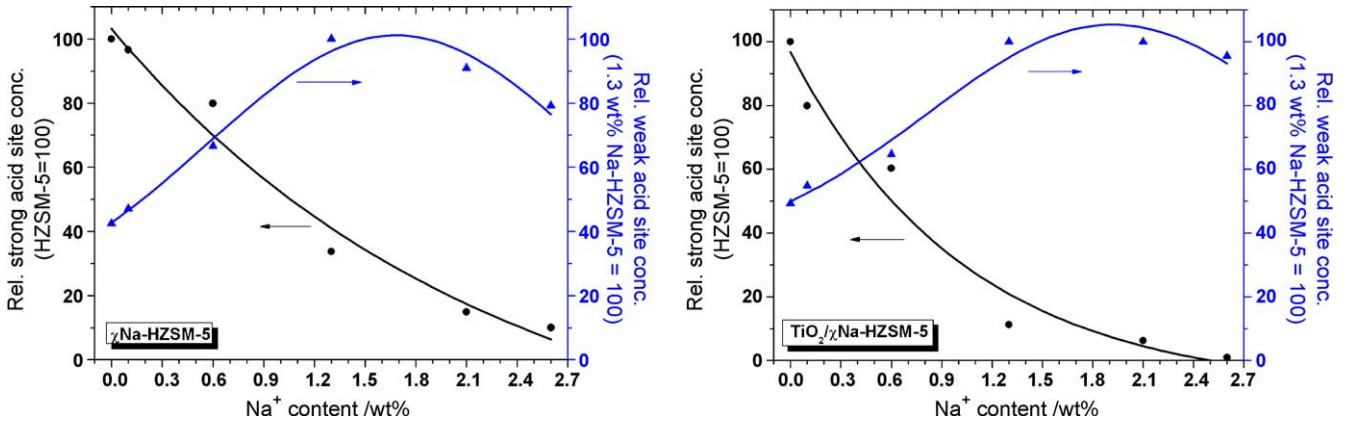

Fig. 10. Plot of strong and weak acid site amounts against the Na^+ content in nano-χNa-HZSM-5 zeolitic supports, where the strong and weak acid site amounts were defined by the integral area of high-temperature peak and low-temperature peak in NH_3-TPD profiles quantitatively measured, respectively.

amorphous SiO_2 and Al_2O_3 supports did not improve the photocatalytic activity of TiO_2. We assigned this to the lack of proper acid sites for MO adsorption on these oxides.

3.3. Reversibility of MO adsorption on TiO_2/χNa-HZSM-5 nano-composites

Some authors have mentioned that weak adsorption of organic compounds on supports favored the photocatalysis of supported TiO_2 [17,27,33]. This might be interpreted by the relative easiness of subsequent desorption and migration of the substrate molecules from adsorption sites to the photoactive sites. In order to study the effect of adsorption bond strength on the photodegradation of MO substrate, the following experiments were carried out: (1) at 298 K, a given amount of χNa-HZSM-5 zeolitic support was put into 100 ml MO solution of 20 mg/l concentration. Under magnetic agitation, the catalyst was allowed 1 h time for adsorption equilibrium. Then the MO-absorbed sample was recovered by vacuum filtration and put into 100 ml deionized water for repeated desorption investigation; each desorption lasted 1 h under agitation. The results were shown in Fig. 15. (2) A given amount of nano-composite photocatalyst was put into 100 ml MO solution of 20 mg/l concentration. Then the

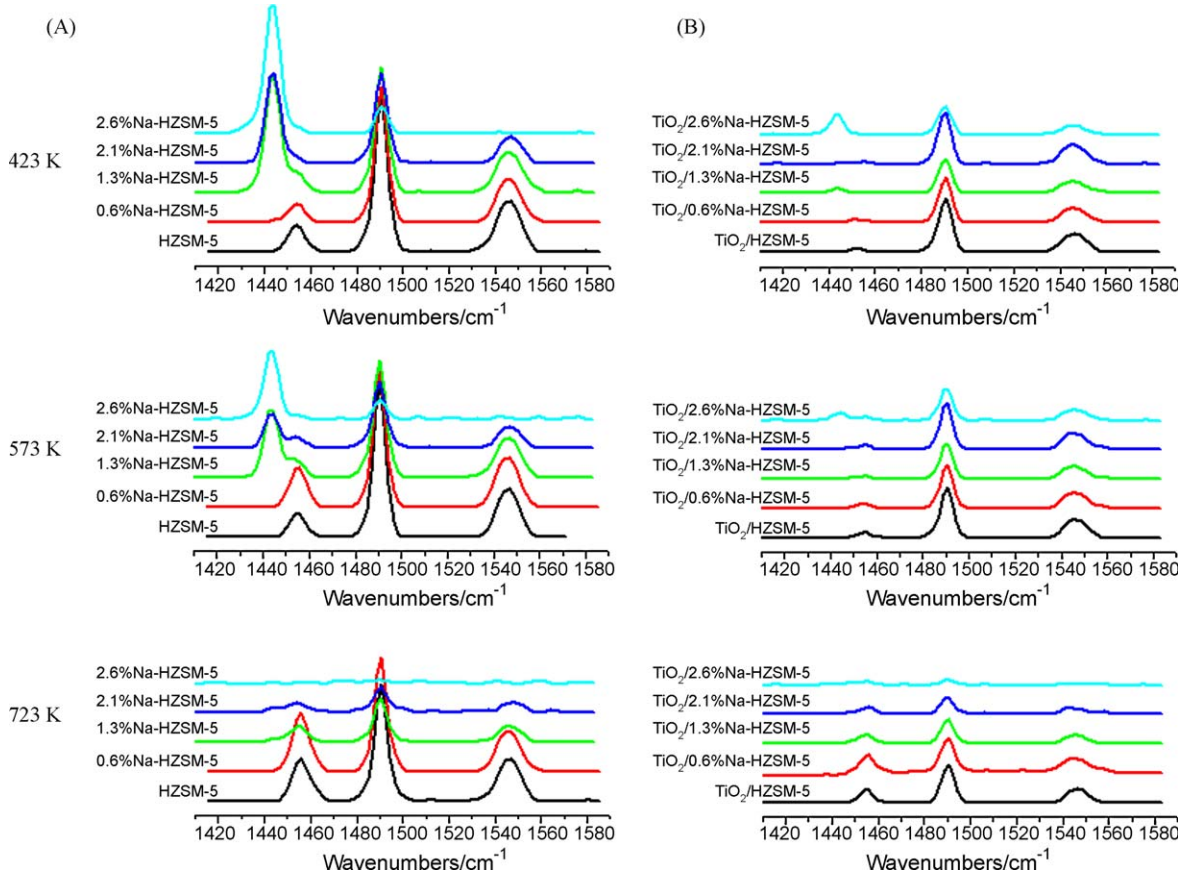

Fig. 11. Pyridine adsorption FT-IR spectra of nano-χNa-HZSM-5 (A) and TiO_2/χNa-HZSM-5 nano-composites (B) at the outgassing temperatures of 423 K, 573 K and 723 K, respectively.

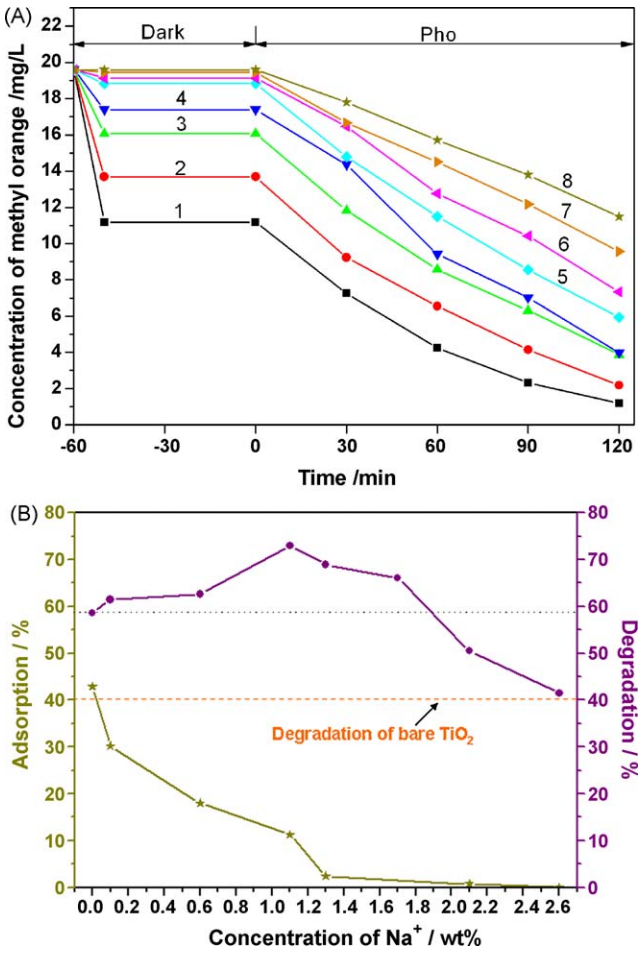

Fig. 12. Effect of Na^+ contents on the adsorption and degradation of MO over TiO_2/χNa-HZSM-5 nano-composites (from 1 to 8, χ = 0, 0.1, 0.6, 1.1, 1.3, 1.7, 2.1, and 2.6 wt.%, respectively). Reaction conditions: initial concentration of MO solution = 20 mg/l, catalyst amount = 1 g/100 ml, temperature = 298 K, irradiation time = 2 h.

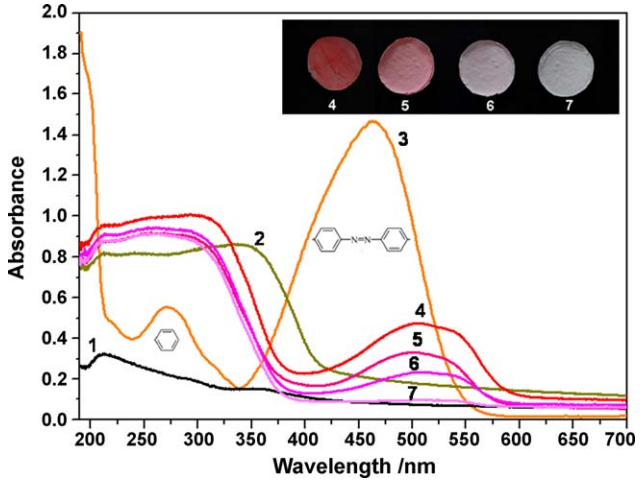

Fig. 13. DRUV–vis spectra of nano-HZSM-5 (1), self-prepared TiO_2 (2), 20 mg/l MO solution (3), and MO-adsorbed TiO_2/χNa-HZSM-5 (from 4 to 7, χ = 0, 0.6, 1.1, and 2.6 wt.%, respectively). Insert: photographs of TiO_2/χNa-HZSM-5 nano-composites adsorbing MO.

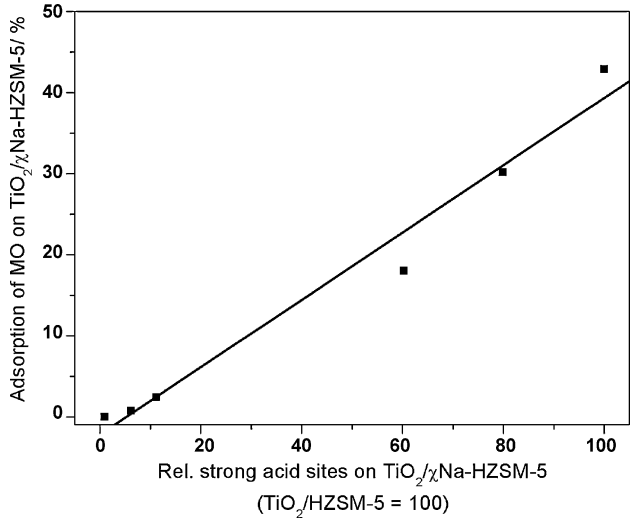

Fig. 14. Plot of MO adsorption capacity of TiO_2/χNa-HZSM-5 against the nano-composites' strong acid site amount.

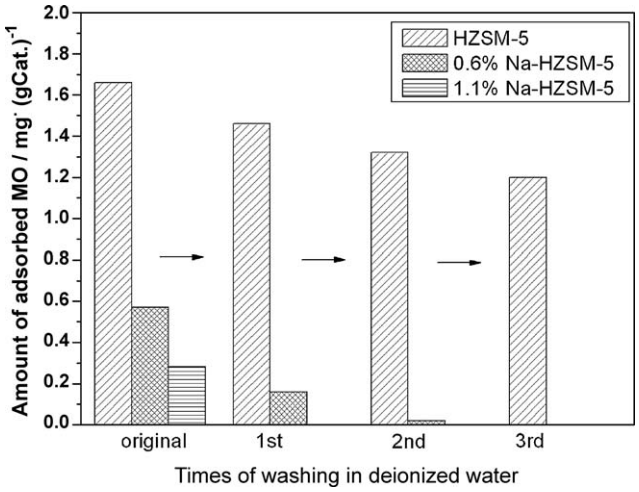

Fig. 15. Desorption of MO from χNa-HZSM-5 zeolitic supports in deionized water at 298 K.

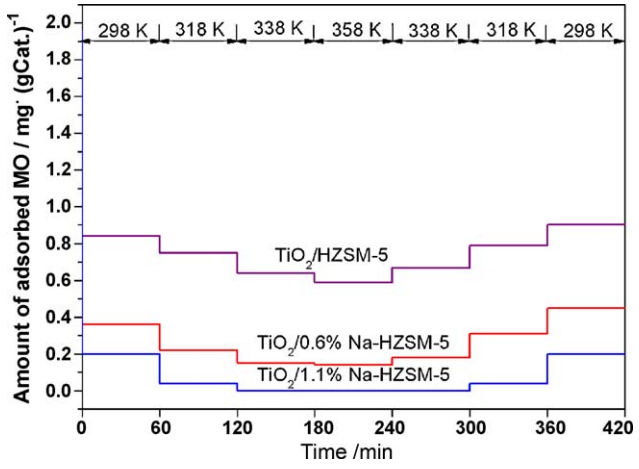

Fig. 16. Reversible adsorption of MO on different TiO_2/χNa-HZSM-5 nano-composite photocatalysts.

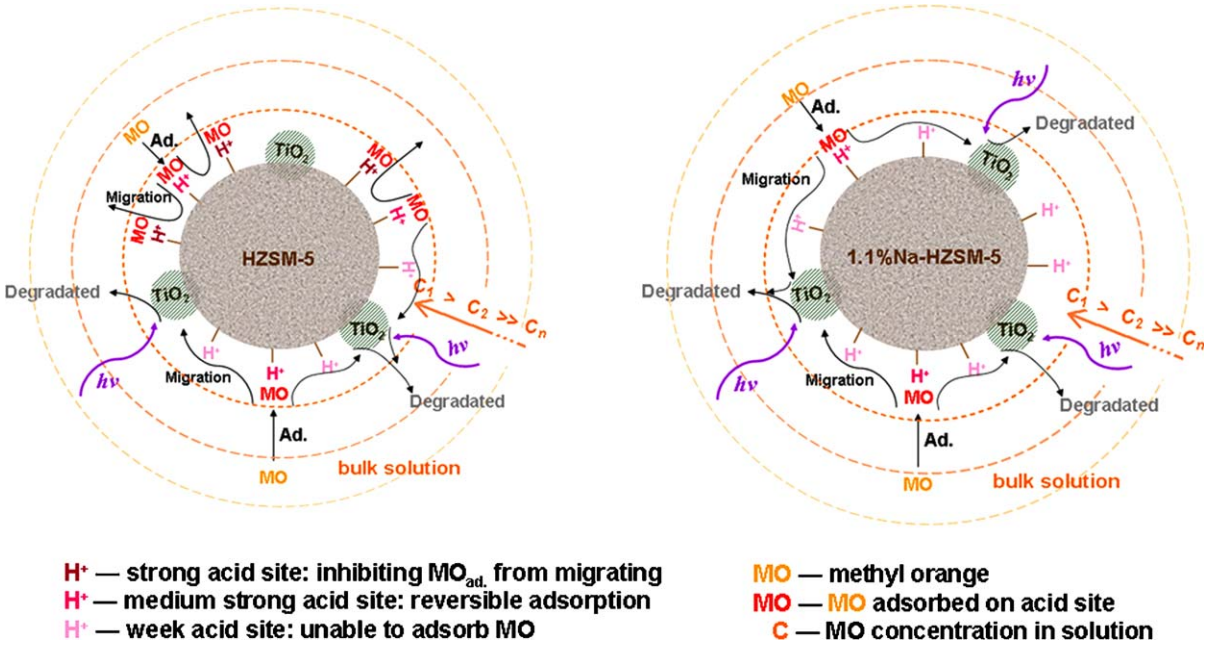

Fig. 17. Scheme of reversible adsorption of MO on TiO_2/HZSM-5 and TiO_2/1.1%Na-HZSM-5 nano-composite photocatalysts.

slurry was magnetically agitated for 1 h at 298 K, 318 K, 338 K and 358 K, respectively. At the end of each hour's agitation, sampling was made to analyze the equilibrium concentration of MO solution. Such operations were repeated following a downward temperature mode at the same temperature levels. Results were depicted in Fig. 16. From Fig. 15 it can be seen that the MO molecules absorbed on the nano-HZSM-5 ($\chi = 0$) are hard to desorb. As the Na^+ content in the nano-supports increasing, the total MO adsorption capacity decreases; however, the desorption of MO becomes easier. For example, during the first time washing in deionized water, approximately 0.2 mg $(gCat.)^{-1}$ MO is desorbed from HZSM-5 into water, accounting for 12.0% of the total adsorption capacity. These values increase to 0.4 mg $(gCat.)^{-1}$ and 71.9% in 0.6% Na-HZSM-5, and 0.3 mg $(gCat.)^{-1}$ and 100% in 1.1% Na-HZSM-5, respectively. From Fig. 16 it can be further seen that, on TiO_2/HZSM-5 nano-composite photocatalysts ($\chi = 0$) only a small percentage of the absorbed MO molecules is permitted to undergo reversible adsorption within 358 K. Especially, the percentage of the reversibly absorbed MO molecules is rather small at lower temperature (ca. 298 K). As the Na^+ contents of the TiO_2/χNa-HZSM-5 nano-composite photocatalysts increasing, however, a higher percentage of MO absorbed on the nano-composite photocatalysts can undergo reversible adsorption, and the reversible adsorption can occur more easily at lower temperature. It is worth noticing that the adsorption of MO molecules on TiO_2/1.1%Na-HZSM-5 nano-composite photocatalyst is nearly completely reversible, and the reversibly absorbed MO molecules are relatively more at lower temperature (ca. 298 K). From the foregoing section we know that TiO_2/1.1%Na-HZSM-5 nano-composite is the best photocatalyst for MO degradation. Based on these results, we conclude that the reversible adsorption of MO on medium strong acid sites promotes MO photodegradation. It is true that the catalyst like TiO_2/0.6%Na-HZSM-5 is comparable with TiO_2/1.1%Na-HZSM-5 in the amount of reversible adsorption sites for MO, but TiO_2/0.6%Na-HZSM-5 has much lower photodegradation activity for MO. We attribute this to the strongly adsorbed MO molecules on the strong acid sites. In the cases of TiO_2/HZSM-5 and TiO_2/0.6%Na-HZSM-5, the strongly adsorbed MO molecules on the strong acid sites would inhibit those reversibly adsorbed MO molecules from migrating along the surface to TiO_2 photocatalytic sites, as shown in Fig. 17.

4. Conclusions

TiO_2 was selectively dispersed on the external surface of a series of nano-sized Na-HZSM-5 zeolitic supports with different Na^+ contents. The large external surface area of the nano-zeolite was found to be able to give high TiO_2 dispersion (less than 10 nm) at a big TiO_2 loading, while leaving considerable free areas for methyl orange adsorption. The nano-sized Na-HZSM-5 supports loaded with TiO_2 had anatase structure, the ultraviolet photo-response of which was dramatically intensified. The modification of support by Na^+ did not affect the loading and dispersion of TiO_2 on the nano-zeolitic supports. However, very significant effects of Na^+ modification were seen on tailoring the acidity of the protonic nano-zeolitic support, and on adjusting the adsorption behavior of the nano-zeolitic supports towards MO substrate. The adsorption of MO took place mainly on the external surface of the supports; the adsorption sites were strong and medium strong acid sites. MO molecules absorbed by strong acid sites were difficult to desorb, while those absorbed by medium strong acid sites were reversible between adsorption and desorption. These adsorptions made MO molecular structure change from azo to quinoid, corresponding to its color change from yellow to red. Na^+-modification attenuated the acidity of the nano-zeolitic support by selectively eliminating stronger acid sites. Therefore, by gradually increasing the Na^+ contents of the nano-zeolitic supports, the amount of strong acid sites of the support decreased preferentially, which was accompanied by the reduction of strongly absorbed MO and the relative increase of reversibly absorbed MO. When the Na^+ content of the support was high enough, both strong and medium strong acid sites of the support were eliminated, so that no MO adsorption was observed (the color of the nano-composite kept white). Generally, the MO photodegradation activities of TiO_2/χNa-HZSM-5 nano-composites were better than that of bare TiO_2. However, they changed remarkably with the Na^+ contents of the supports, giving the maximum value at $\chi = 1.1$ wt.% when the adsorption of MO by nano-zeolitic support was nearly completely reversible, and giving the minimum value, equivalent to that of the bare TiO_2, at $\chi = 2.6$ wt.% when the nano-zeolitic support had no ability to absorb MO substrate, just like the bare TiO_2. These results

highlight the significance of the reversible adsorption of the substrate by support in promoting the photocatalytic activity of supported TiO_2.

Acknowledgement

This work is financially supported by the Foundation for Talented Scholars from Liaoning province, China.

References

[1] M. Matsuoka, M. Anpo, J. Photochem. Photobiol. C: Photochem. Rev. 3 (2003) 225–252.
[2] S. Anandan, M. Yoon, J. Photochem. Photobiol. C: Photochem. Rev. 4 (2003) 5–18.
[3] A. Corma, H. Garcia, Chem. Commun. (2004) 1443–1459.
[4] M. Kitano, M. Matsuoka, M. Ueshima, M. Anpo, Appl. Catal. A: Gen. 325 (2007) 1–14.
[5] C. Ooka, H. Yoshida, M. Horio, K. Suzuki, T. Hattori, Appl. Catal. B: Environ. 41 (2003) 313–321.
[6] C. Wu, L. Tzeng, Y. Kuo, C.H. Shu, Appl. Catal. A: Gen. 226 (2002) 199–211.
[7] S. Sakthivel, M.V. Shankar, M. Palanichamy, B. Arabindoo, V. Murugesan, J. Photochem. Photobiol. A: Chem. 148 (2002) 153–159.
[8] R.J. Tayade, R.G. Kulkarni, R.V. Jasra, Ind. Eng. Chem. Res. 46 (2007) 369–376.
[9] F. Li, S. Sun, Y. Jiang, M. Xia, M. Sun, B. Xue, J. Hazard. Mater. 152 (2008) 1037–1044.
[10] H.-J. Nam, T. Amemiya, M. Murabayashi, K. Itoh, J. Phys. Chem. B 108 (2004) 8254–8259.
[11] Y. Chen, D.D. Dionysiou, J. Mol. Catal. A: Chem. 244 (2005) 73–82.
[12] N. Takeda, T. Torimoto, S. Sampath, S. Kuwabata, H. Yoneyama, J. Phys. Chem. 99 (1995) 9986–9991.
[13] Y. Xu, W. Zheng, W. Liu, J. Photochem. Photobiol. A: Chem. 122 (1999) 57–60.
[14] M.M. Mohamed, T.M. Salama, T. Yamaguchi, Colloids Surf. A 207 (2002) 25–32.
[15] A.A. Ismail, I.A. Ibrahim, M.S. Ahmed, R.M. Mohamed, H. El-Shall, J. Photochem. Photobiol. A: Chem. 163 (2004) 445–451.
[16] Z. Pi, L. Cai, J. Zhong, M. Gong, Y. Chen, Chin. J. Catal. 29 (2008) 453–457.
[17] H. Yoneyama, T. Torimoto, Catal. Today 58 (2000) 133–140.
[18] J. Shi, J. Zheng, P. Wu, X. Ji, Catal. Commun. 9 (2008) 1846–1850.
[19] N. Takeda, N. Iwata, T. Torimoto, H. Yoneyama, J. Catal. 177 (1998) 240–246.
[20] J. Matos, J. Laine, J.M. Herrmann, Appl. Catal. B: Environ. 18 (1998) 281–291.
[21] C.H. Ao, S.C. Lee, J. Photochem. Photobiol. A: Chem. 161 (2004) 131–140.
[22] Y. Yu, J.C. Yu, C.-Y. Chan, Y.-K. Che, J.-C. Zhao, L. Ding, W.-K. Ge, P.-K. Wong, Appl. Catal. B: Environ. 61 (2005) 1–11.
[23] B. Liu, H.C. Zeng, Chem. Mater. 20 (2008) 2711–2718.
[24] B. Sun, E.P. Reddy, P.G. Smirniotis, J. Catal. 237 (2006) 314–321.
[25] E.P. Reddy, L. Davydov, P. Smirniotis, Appl. Catal. B: Environ. 42 (2003) 1–11.
[26] M. Noorjahan, V. Durga Kumari, M. Subrahmanyam, P. Boule, Appl. Catal. B: Environ. 47 (2004) 209–213.
[27] G. Li, X.S. Zhao, M.B. Ray, Sep. Purif. Technol. 55 (2007) 91–97.
[28] A. Corma, Chem. Rev. 97 (1997) 2373–2419.
[29] Y. Xu, C.H. Langford, J. Phys. Chem. 99 (1995) 11501–11507.
[30] Y. Xu, C.H. Langford, J. Phys. Chem. 101 (1997) 3115–3121.
[31] H. Yamashita, K. IKeue, T. Takewaki, M. Anpo, Top. Catal. 18 (2002) 95–100.
[32] V. Durgakumari, M. Subrahmanyam, K.V. Subba Rao, A. Ratnamala, M. Noorjahan, K. Tanaka, Appl. Catal. A: Gen. 234 (2002) 155–165.
[33] M.V. Shankar, K.K. Cheralathan, B. Arabindoo, M. Palanichamy, V. Murugesan, J. Mol. Catal. A: Chem. 223 (2004) 195–200.
[34] F. Li, Y. Jiang, L. Yu, Z. Yang, T. Hou, S. Sun, Appl. Surf. Sci. 252 (2005) 1410–1416.
[35] M.V. Shankar, S. Anandan, N. Venkatachalam, B. Arabindoo, V. Murugesan, Chemosphere 63 (2006) 1014–1021.
[36] N. Dubey, S.S. Rayalu, N.K. Labhsetwar, R.R. Naidu, R.V. Chatti, S. Devotta, Appl. Catal. A: Gen. 303 (2006) 152–157.
[37] H. Yahiro, T. Miyamoto, N. Watanabe, H. Yamaura, Catal. Today 120 (2007) 158–162.
[38] M. Takeuchi, T. Kimura, M. Hidaka, D. Rakhmawaty, M. Anpo, J. Catal. 246 (2007) 235–240.
[39] W. Panpa, P. Sujaridworakun, S. Jinawath, Appl. Catal. B: Environ. 80 (2008) 271–276.
[40] L.P. Hammett, A.J. Deyrup, Acidity Functions of Sulfuric and Perchloric Acids 54 (1932) 2721–2739.
[41] M.W. Anderson, J. Klinowshi, Zeolites 6 (1986) 150–153.
[42] X.Q. Wang, X.S. Wang, X.W. Guo, CN Patent 99102700.0 (1999).
[43] C.J. Ren, B.H. Zhong, H. Liu, Y.X. Zhang, J. Chem. Eng. Chin. Univ. 18 (2004) 57–61.
[44] E. Vaisman, R.L. Cook, C.H. Langford, J. Phys. Chem. B 104 (2000) 8679–8684.
[45] S. Zheng, L. Gao, Q. Zhang, W. Zhang, J. Guo, J. Mater. Chem. 11 (2001) 578–583.
[46] J. Klaas, G. Schulz-Ekloff, N.I. Jaeger, J. Phys. Chem. B 101 (1997) 1305–1311.
[47] M.M.J. Treacy, J.B. Higgins, Collection of Simulated XRD Powder Patterns for Zeolites, fourth ed., Elsevier, 2001.
[48] A. Henlein, Chem. Rev. 89 (1989) 1861–1873.